ADVANCED OPTICAL MATERIALS
www.advopticalmat.de

Planar Photonic Crystal Biosensor for Quantitative Label-Free Cell Attachment Microscopy

*Weili Chen, Kenneth D. Long, Jonas Kurniawan, Margaret Hung, Hojeong Yu, Brendan A. Harley, and Brian T. Cunningham**

In this study, a planar-surface photonic crystal (PC) biosensor for quantitative, kinetic, label-free imaging of cell–surface interactions is demonstrated. The planar biosensor surface eliminates external stimuli to the cells caused by substrate topography to more accurately reflect smooth surface environment encountered by many cell types in vitro. Here, a fabrication approach that combines nanoreplica molding and a horizontal dipping process is used to planarize the surface of the PC biosensor. The planar PC biosensor maintains a high detection sensitivity that enables the monitoring of live cell–substrate interactions with spatial resolution sufficient for observing intracellular attachment strength gradients and the extensions of filopodia from the cell body. The evolution of cell morphology during the attachment and spreading process of 3T3 fibroblast cells is compared between planar and grating-structured PC biosensors. The planar surface effectively eliminates the directionally biased cellular attachment behaviors that are observed on the grating-structured surface. This work represents an important step forward in the development of label-free techniques for observing cellular processes without unintended external environmental modulation.

1. Introduction

The critical role of the interactions between cells and their microenvironment upon directing and controlling cell behavior within the context of a diverse set of cellular processes has been extensively studied due to promising applications in tissue engineering, regenerative medicine, and preclinical pharmaceutical analysis.[1–3] Importantly, the spatial and temporal dynamics of cell–surface interactions are a fundamental aspect of the biology of how cells communicate with their environment. Total internal reflectance fluorescence microscopy and confocal fluorescence microscopy have been the most widely used tools for visualization of cell–surface interactions through the use of fluorescent dyes that can be specifically targeted to bind with membrane components.[4,5] Although detailed information about cell adhesion activity can be provided by these methods, the rapid rate of fluorophore photobleaching poses a severe practical restriction upon the period during which the cells can be observed, and is not capable of quantification of the engagement between the cell and the surface it is attached to. Therefore, fluorescence imaging is not suitable for long-term monitoring of cells, especially for extremely important activities that occur over extended time scales, such as cell differentiation, metastasis, and chemotaxis.[6]

Label-free biosensors have been developed that are able to overcome the inherent challenges in the label-based cell detection methods to provide noninvasive and nondestructive measurements of cell behavior.[7–9] Instead of relying upon fluorescent tags, label-free biosensors are designed to measure an intrinsic property of cells, such as dielectric permittivity, mass, or electrical impedance. For example, biosensor technologies using prism coupler-based and grating coupler-based surface plasmon resonance (SPR) are capable of detecting cell attachment between a metal surface and the membrane proteins in living cells.[10,11] Electrical sensing approaches have also been reported to provide label-free detection of cells by tracking the electrical conductivity distribution within cells upon a microelectrode-covered substrate.[12] Biosensor-based detection of cell–surface interactions is especially desirable when the transducer surface only responds to cell attachment events that occur at the transducer–cell interface (and thus measure the strength

W. Chen, H. Yu, Prof. B. T. Cunningham
Department of Electrical and Computer Engineering
University of Illinois at Urbana-Champaign
Urbana, IL 61801, USA
E-mail: bcunning@illinois.edu
K. D. Long, Prof. B. T. Cunningham
Department of Bioengineering
University of Illinois at Urbana-Champaign
Urbana, IL 61801, USA
J. Kurniawan
Department of Materials Science and Engineering
University of Illinois at Urbana-Champaign
Urbana, IL 61801, USA
M. Hung
School of Molecular and Cellular Biology
University of Illinois at Urbana-Champaign
Urbana, IL 61801, USA
Prof. B. A. Harley
Department of Chemical and Biomolecular Engineering
University of Illinois at Urbana-Champaign
Urbana, IL 61801, USA
Prof. B. A. Harley
Institute for Genomic Biology
University of Illinois at Urbana-Champaign
Urbana, IL 61801, USA

DOI: 10.1002/adom.201500260

of engagement of the cell membrane with the surface) rather than sensing the bulk properties of the cell. Only a few of the label-free biosensing approaches have the capability of imaging cell–surface interactions. In particular, SPR imaging and photonic crystal enhanced microscopy (PCEM) have demonstrated the ability to generate images of the magnitude of cell–surface attachment with subcell spatial resolution,[13–15] and PCEM is the only approach to demonstrate submicron spatial resolution using a low-magnification (10×) objective.[16,17]

Photonic crystal (PC) biosensors have been demonstrated as a versatile platform for a wide range of label-free biological assays including DNA microarrays, virus sensing, cell attachment characterization, and high throughput drug screening.[16,18–22] The structure used in this work is a 1D PC slab with alternating high and low refractive index layers, with a grating period smaller than the wavelength of the resonantly coupled light. For such subwavelength grating structures, the zeroth diffracted orders propagate while all higher orders are cut off, resulting in a characteristic photonic band gap that does not occur in an ordinary diffraction grating. Upon illumination with polarized light at normal incidence, constructive interference of the out-coupled light with the backward diffracted zeroth order and destructive interference with the forward diffracted zeroth order yields a sharp resonant reflection peak with nearly 100% reflection efficiency. The structure used in this work exhibits a bandgap for light polarized perpendicular to the grating lines as the reflection efficiency varies with the angle of light incident, as shown in ref. [23]. As biomaterials attach to the PC surface and increase the effective refractive index within the evanescent field region, the resonant wavelength shifts to larger values. Biosensing is performed by measuring shifts in the peak wavelength value (PWV) of the reflection spectrum (see Figure S1, Supporting Information). Importantly, the resonant electromagnetic field standing wave does not propagate laterally across the PC surface, so that a localized change in effective refractive index only changes the PWV at one point on the PC surface without changing the PWV in the surrounding area. By measuring changes in PWV on a pixel-by-pixel basis on a PC surface with ≈0.5 μm pixel resolution, PCEM has been demonstrated as a powerful tool for quantification and imaging of cell–surface interactions under the circumstances of complex cellular activities such as chemotaxis and drug-induced apoptosis.[16,24] By virtue of the surface-confined evanescent waves generated by the PC biosensor at the resonant condition, PCEM can probe cell activity that is localized to the interface between the cells and their substrate. The spatial resolution of PCEM label-free imaging is dictated by the lateral propagation of the resonant electromagnetic field standing wave.[17] The asymmetry of the grating structure results in slightly different propagation lengths for resonantly coupled light in the two orthogonal directions parallel to the PC surface as quantified in a previous publication.[25] The PC's ability to strictly limit lateral propagation of resonantly coupled light enables near real-time, spatially resolved detection of fine-structured filopodia, and intracellular attachment strength gradients. Dynamic information about evolution of cell focal adhesions, cell–surface attachment morphology, and cell attachment gradients within individual cells can be provided over biologically relevant time scales without the use of fluorescent labels or colored stains.[16,24,26–28]

An important emerging issue for the application of surface-structured biosensors to label-free cellular detection is the topography of the biosensor surfaces which, although serving as a substrate for cellular activity, can introduce external stimuli to the adherent cells, and activate cellular functions that would not normally occur on a planar surface.[29,30] Considering that most cells are anchorage dependent and collect information from their surrounding environment to orient, move, and differentiate, substrate topography is a critical factor for a variety of surface-based cellular activities.[31] Particularly, topographic structures at the submicron scale have been intensively reported as a means to intentionally induce specific cell behavior, as they exist in the same length scale as extracellular matrix (ECM) structures. The contact guidance provided by surface structures has been found to affect cell adhesion strength, alter cell morphology, stimulate cell proliferation, initiate intracellular signaling, and regulate stem cell differentiation.[32] Although cell–topography interactions vary across different cell types, substrate materials, and surface features, there are some common trends for many kinds of mammalian cells. Periodic grating structures comprise one of the most commonly studied features in cell–surface research, upon which many cell types, including stem cells, epithelial cells, endothelial cells, smooth muscle cells, and Schwann cells, typically respond to the surface structure by simultaneously aligning and extending themselves along the grating axis.[33] Enhanced responses can be produced by cells cultured on grating substrates with decreased pitch and increased depth in the nanometer to micrometer range.[34] The phenomena that usually co-occur with cell morphology alteration are biased cell migration following the grating lines and increased average migration speed. These behaviors may be caused by the inhomogeneous distribution of adhesion molecules and leading protrusions that are induced by the nonuniform contacts between cells and their patterned substrates.[35] Cell–substrate interactions with other types of substrate topologies including pillars, pores, spheres, cylinders, and pyramids have also been studied and demonstrate evident surface modulation effects upon cell activity.[36]

In situations for which a biosensor surface must be designed to provide nondisturbing measurements of natural cell behavior in environments that mimic nonstructured surfaces encountered in vitro, it is highly desirable to provide a transducer surface that is substantially flat. Observation of cell behavior such as adhesion, migration, and cytoskeletal organization on a planar biosensor substrate can represent cell behavior that is equivalent to those that occur upon commonly used glass slides in most microscopy approaches. As the basis of most cell in vitro work that is performed upon the unpatterned surfaces of microscope slides, microtiter plates, and microfluidic devices, a planar surface enables many existing cell assay methodologies to be employed, and is a building block for a wide array of surface modification techniques that are used to intentionally modify cellular attachment shapes and strengths during common biological processes.[37–39]

Facilitated by the development of semiconductor technologies, surface planarization can be achieved through polishing techniques such as chemical-mechanical-planarization or coating techniques such as spin coating.[40,41] Recently, a novel surface planarization approach called "horizontal dipping" has

Adv. Optical Mater. 2015,
DOI: 10.1002/adom.201500260

been demonstrated as an effective method for the fabrication of large-area-distributed feedback lasers on plastic substrates.[42] Horizontal dipping is a solution-phase coating method that allows for large-area, high-uniformity, and thin-film polymer deposition onto device surfaces with nanometer-level precision for <200 nm thin films. Horizontal dipping planarization is performed at room temperature and does not need substrate rotation. In the horizontal dipping process, a curtain-like liquid polymer solution for coating is maintained by capillary action within the gap space between the device surface and a horizontal rod placed closely above the surface. The rod can be translated horizontally to lead the motion of the solution and help the solution to be evenly spread onto the device surface. Due to the surface tension within the liquid precursor, the surface of the coated layer can be uniformly flat over a large area. The thickness of the polymer layer is determined by the process parameters set in the dipping process, such as gap height, translation speed, and liquid viscosity, and it can be flexibly modulated by changing these parameters.[43] These properties make horizontal dipping an ideal method for creating an extremely thin and planar polymer layer on top of the grating structures of a PC surface.

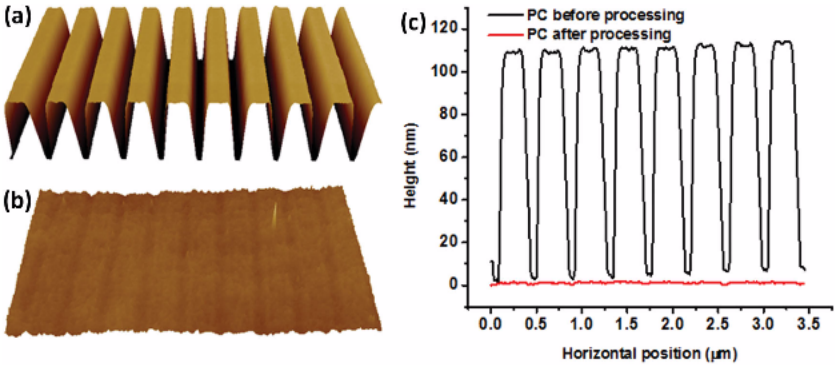

Figure 1. AFM measurements of the PC before and after planarization. a) The PC before horizontal dipping exhibits surface topography of a grating structure, with a grating depth of 105 nm and a grating period of 400 nm. b) However, after the planarization process a flat surface with topography (<1 nm) barely measurable by AFM is obtained. c) Cross-section profile plots of both surfaces are shown together on the same scale.

In this paper, we report the first implementation of a planar PC biosensor for label-free imaging of live cells, which enables PCEM imaging of cell–surface interactions with high spatial and temporal resolution. We fabricate the planar PC biosensor on standard glass coverslips through a process that combines polymer nanoreplica molding and horizontal dipping, which enables PC biosensors to be easily incorporated into microscope slides or microplates that are typically used for cell biology research. The planar surface of the label-free PC biosensor enables the monitoring of the natural behaviors of cells, avoiding the interference brought by the topographic structures. High detection sensitivity is maintained by the planar PC through the efficient coupling between the surface-confined evanescent waves and the observed cells. Here, we demonstrate label-free time-lapse imaging of adhesion and migration processes of 3T3 fibroblast cells that are cultured on the PC surface over an extended time period. PCEM can clearly identify the subtle variation in cell adhesion strength within a single cell, the extension of the filopodial and morphological variations during migration, demonstrating significant potential for the further investigation of a variety of cellular processes such as stem cell differentiation, invasion, chemotaxis, and apoptosis. Critically, these studies can be performed on selected ECM proteins that are coated on top of the PC surface, facilitating the direct investigation of the chemistry of cell–matrix interactions.

2. Results

2.1. PC Surface Characterization

To examine the surface profile of the planar PC biosensor and demonstrate the effectiveness of the planarization process, atomic force microscopy (AFM; Digital Instruments Dimension 300) is used to characterize the PC surface before the horizontal dipping process and after the final deposition of TiO_2. A standard silicon nitride AFM cantilever is used in this study. Data are acquired by scanning over an area of 4×2 μm^2 on 128 pixel lines at a scan rate of 1.0 Hz, and 256 imaged points are collected at each scanned line. The measurement results are shown in **Figure 1**.

The surface morphology of the PC before horizontal dipping is shown in Figure 1a, where the arrangement of grooves across the PC surface demonstrates excellent uniformity of the nanoreplica molding process. As measured by AFM, the PC surface structure reflects the geometry of the molding template, with a grating period of 400 nm and a grating depth of 105 nm, which is slightly lower than the depth of the template due to the sidewall deposition effect of sputter coating. However, after the planarization process, the topographic structures on the PC surface are completely eliminated as shown in Figure 1b. AFM measurements show that depth variation of the planarized PC is less than 1 nm, with a surface roughness of 0.58 nm over the entire PC area (Figure 1c). The flat surface of the PC obtained through the planarization process thus provides an ideal label-free sensing platform for the detection cell–surface interactions that are not biased by a surface structure.

The reflection spectrum, as an important indicator of the optical properties of the PC biosensor, is recorded after the addition of three successive material coating steps. Polarized white light (polarization axis perpendicular to the PC grating lines) is used to illuminate the PC surface at normal incidence from below. The measurements are performed while the PC surface is immersed in water. **Figure 2**b shows that the resonant wavelength of the PC after the initial TiO_2 deposition is 603 nm and the full width at half maximum (FWHM) is $\Delta\lambda = 2.1$ nm. After the polymer coating, horizontal dipping, and etchback, the change in the effective refractive index of the superstrate (in which water in the grating teeth is replaced by SU-8) causes a positive shift of the PWV to $\lambda = 612$ nm. Concurrently, the FWHM decreases to $\Delta\lambda = 1.9$ nm due to the small drop of the refractive index contrast within the PC structure. To optimize the coupling efficiency of the incident LED light

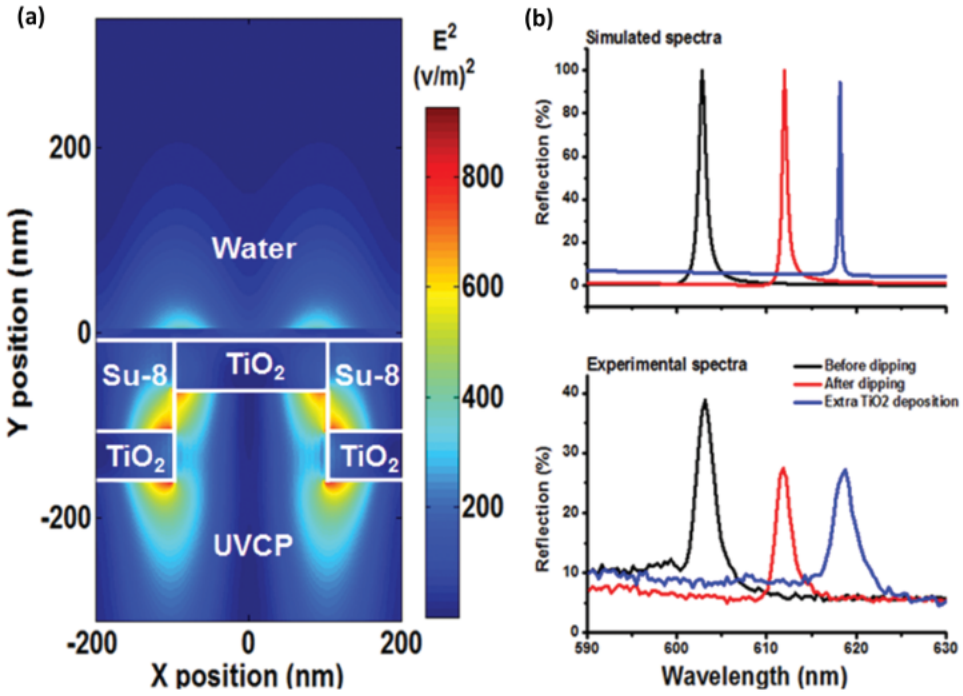

Figure 2. a) RCWA simulation of the electric field distribution of the planar PC illuminated at the resonance condition. b) Comparison between simulated and measured reflection spectra of the PC after three successive material coating processes: the initial sputtering coating, the SU-8 coating, and the final sputtering coating.

(λ_{peak} = 617 nm) with the PC structure, the final resonant wavelength of the device is designed to occur at λ = 619 nm through the addition of the TiO_2 thin film. The high refractive index coating effectively increases the PWV and broadens the FWHM to $\Delta\lambda$ = 2.5 nm. These results show that the planarized PC maintains a resonant reflection spectral linewidth that is similar to its unplanarized counterpart for biosensing applications.

2.2. Rigorous Coupled Wave Analysis Simulation

We use rigorous coupled wave analysis (RCWA) simulations of the planar PC structure to evaluate the influence of the planarization process on the sensitivity performance and to visualize the redistribution of electromagnetic fields (Figure 2a).[45] One period of the PC structure is simulated, with periodic boundary conditions applied in the direction perpendicular to the grating lines. The physical dimensions of the modeled structures are derived from measured quantities in the fabricated device. In order to mimic the aqueous environment of cell imaging experiments, the superstrate material of the PC is chosen to represent water with a refractive index of n_{water} = 1.33. Under illumination from a uniform plane wave at normal incidence, the RCWA simulation predicts a resonant reflection wavelength of λ = 618 nm and a reflection efficiency of η_R = 94%. The spatial distribution of the near-field electric field (normalized to the intensity of the incident field) at the resonant wavelength is shown in Figure 2a. The intensity of the electric field is indicated in the figure to show the decay of the electric field magnitude of the evanescent field with respect to increasing distance from the interface. The resonant electromagnetic standing waves generate a high-intensity surface-bound electric field with magnitudes as high as $|E|^2$ = 800 (V m^{-1})^2 in proximity to the TiO_2 layer, especially around the corners of the grooves.[46] Although the SU-8 polymer filling into the grating gaps pulls the high field intensity region away from the upper surface that is exposed to the cells, the evanescent tails of the resonant electric field are still capable of penetrating into the superstrate material to sense the biomaterials attached to the PC surface. We also observe that the presence of the thin TiO_2 film with high refractive index on the PC surface serves to improve the optical confinement of the resonance mode. The fraction of the electrical field that overlaps with the cells, according to the simulation, penetrates ≈200 nm into the cellular material, enabling the planar PC to probe the cell–surface interactions that only occur at the interface between the cell and its substrate. A positive peak wavelength shift is generated through the replacement of the aqueous cell media with cellular material that occupies the evanescent field, resulting from the fact that the refractive index of the cellular materials is larger than that of the cell media. The extent of the evanescent field occupied by the cell and the value of the refractive index of the material engaged with the surface evanescent field are the two major contributors to the magnitude of the PWV shift.

RCWA modeling is also used to calculate the expected far-field resonant reflection spectrum of the planar PC, as shown in Figure 2b. The computer model prediction is in good agreement with the experimental data. The simulated resonant reflection occurs at λ = 603 nm for the PC after the initial deposition of the TiO_2 film (n_{TiO2} = 2.36) with an FWHM of $\Delta\lambda$ = 1 nm. When the grating teeth are completely filled by the polymer (n_{SU-8} = 1.58), the corresponding PWV and FWHM are

Adv. Optical Mater. 2015,
DOI: 10.1002/adom.201500260

$\lambda = 612$ nm and $\Delta\lambda = 0.6$ nm. After the addition of a 10 nm TiO_2 thin film on top of the structure, the resonant wavelength shifts to $\lambda = 618$ nm and the FWHM decreases to $\Delta\lambda = 0.3$ nm. The spectral locations of the simulated resonant wavelengths are highly consistent with values measured from fabricated devices. The discrepancy between the measured and simulated FWHM likely arises because the simulation does not take into account the sidewall deposition of the sputtered film and the FWHM of the optical resonance is near the spectral resolution of the spectrometer used in the measurements.

It should be noted that RCWA simulation predicts a higher reflection efficiency than that measured experimentally for the fabricated PC, and that nonplanarized PC surfaces typically achieve reflection efficiencies of 95%–100% at the resonant wavelength. The discrepancy can be attributed to a small degree of optical absorption of the SU-8 at the resonant wavelength that serves to quench the PC resonance. While absorption reduces the reflection efficiency, it does not impact the sensitivity of the biosensor, as measured by the amount of wavelength shift induced by cell attachment.

2.3. Label-Free Imaging of Cell Attachment and Migration

To characterize the adhesion patterns of live cells to the planar substrate, 3T3 fibroblasts are cultured onto fibronectin-treated PC surfaces and monitored for 5 h. This cell line is selected for its common use throughout the fields of tissue engineering and bioengineering, and because its attachment profile has been thoroughly demonstrated as highly susceptible to substrate topography.[47] A baseline PWV image is gathered before the introduction of cells, when the PC is uniformly covered by cell media. The baseline PWV image is aligned and mathematically subtracted from subsequent PWV images gathered during and after cell attachment, in order to remove any effects of nonuniformity in either PC fabrication or the fibronectin coating processes. This means that the PWV shift relative to the baseline at each pixel position in the subsequent PWV images is caused by the activity of cell attachment upon the PC surface.

As the PC's resonantly reflected wavelength is sensitive to the variation of refractive index within the sensing volume of the evanescent electric field, our approach measures biomaterial mass density near the sensor surface.[48] A positive PWV shift at each pixel position corresponds to a localized increase in the density of cellular material located within the close surrounding region above the pixel area. A variety of cellular behaviors, including cell adhesion, migration, division, endocytosis, and exocytosis, involve the relocation of cellular organelles and biomolecules, such as membrane protein trafficking, cytoskeletal rearrangement, morphological changes, and receptor adhesion.[49]

In order to compare the responsive behaviors of 3T3 fibroblast cells to planar and the nonplanar surfaces of the PC biosensor, dynamic and quantitative information about cell morphology and cell–matrix interaction is gathered by the series of ΔPWV images summarized in **Figure 3** and **Figure 4**. Images presented here are captured every 20 min for a duration of over 5 h. Figure 3 shows the time-lapse label-free images of cellular attachment and spreading processes of 3T3 fibroblast cells on a fibronectin-coated nonplanar PC surface (see Video S1, Supporting Information). An initial attachment pattern can be identified on the first image frame as the small, round areas of positive PWV shift appear as a result of the initial contact between cells coming out of suspension and attaching to the PC surface. As would be expected, the PWV shift is greatest in the center of the attachment of these spheroid cells. During the initial stages of cell–matrix interaction, as shown in the following frames, the cells passively adhere to the PC surface and then start to reshape their morphological profiles while sensing the substrate with thin filopodia which can be seen radiating out from the

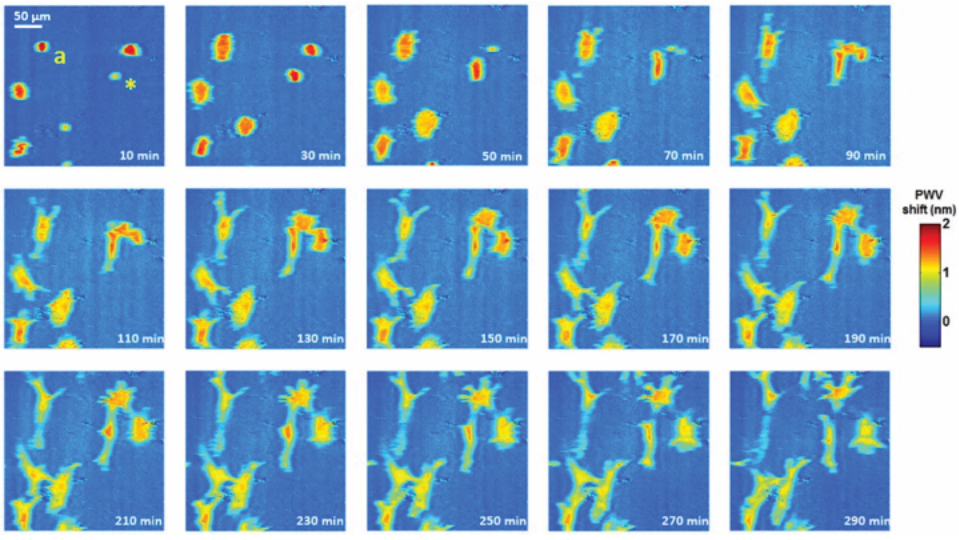

Figure 3. Time-lapse label-free images of cell attachment and migration process of 3T3 fibroblast cells on a fibronectin-coated nonplanar PC surface. Images are shown at 20 min increments over a 5 h time period. Small regions of initial cell attachment appear on the first frame with positive PWV shift. Filopodial extensions can be observed extending in multiple directions as the cells explore the environment. Cellular spreading is eventually established preferentially in the grating direction of the PC after about 2 h.

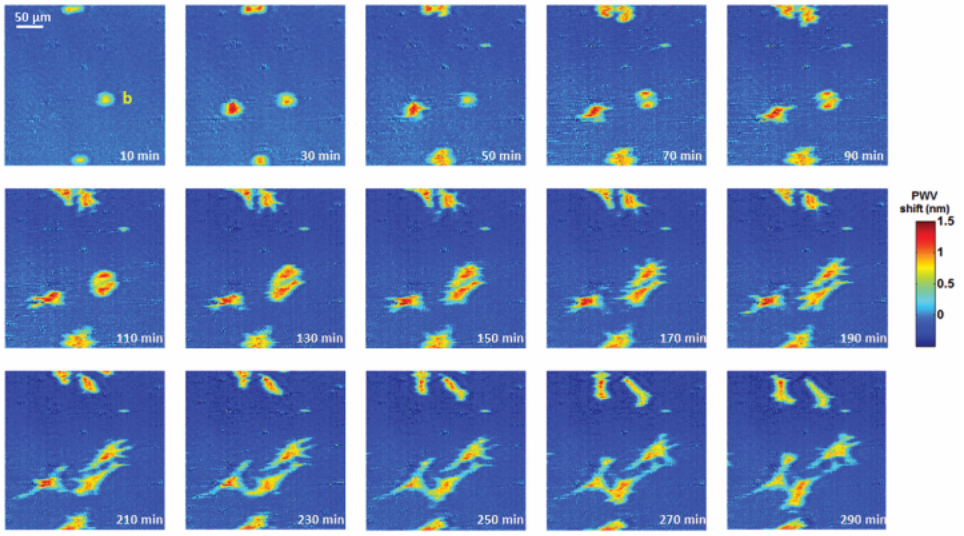

Figure 4. Time-lapse label-free images of cell attachment and migration process of 3T3 fibroblast cells on a fibronectin-coated planar PC surface, with images displayed at 20 min intervals. Similar initial adhesion patterns are observed as obtained upon nonplanar PCs, with multidirectional filopodia extending away from cell bodies after initial attachment followed by cell body spreading. As time progresses, the cells appear to align themselves more randomly, as commonly observed during traditional cell culture on nonpatterned surfaces.

cell body. For example, the marked cell (*) in Figure 3 can be observed attaching in a point-like area, and after 50 min, a small protrusion is observed toward the top of the image (along the grating direction). An increase in both area and magnitude of PWV shift is observed, as the cell body is pulled in that direction. At 110 min, the cell appears to have strongest attachment at two locations at opposite ends of the cell, with this distribution becoming more pronounced through 170 min, consistent with high concentrations of cellular attachment protein at these focal adhesions. By 210 min, the cell appears to be moving in the direction of one of those focal adhesions, and continues to sense and move across the sensor. As time progresses, enhanced alignment and extension of cells are observed specifically along the grating direction (vertical direction on the image) on the nonplanar PC biosensor. The axis of elongation of the majority of observed cell bodies is generally aligned parallel to the grating direction, and many of the filopodial protrusions can be observed extending from cell bodies along that same direction.

Figure 4 shows representative images of the cell attachment and spreading patterns of the same 3T3 fibroblast cells on a planar PC surface that was previously coated with fibronectin. In both cases, intracellular attachment patterns are consistent with those described previously.[16,17] The cells display similar initial attachment patterns in the first frame, compared to what is observed on the nonplanar PC, with higher PWV shifts present in the center of the cell, as the highest concentration of cellular material as a spheroid cell enters the planar evanescent region is a single point. As time progresses, the adhesion area gradually increases, and membrane boundaries become increasingly irregular as cellular processes begin to extend from cell bodies, indicating the formation of focal adhesions used to sense the topography of the extracellular environment.[50]

In contrast to the biased morphology of cells on a nonplanar PC surface, no preferential orientation or elongation is observed during the long-term monitoring of cellular attachment and subsequent migration on the planar PC surface. A time-lapse movie of the entire adhesion and migration process is shown in Video S2 (Supporting Information) that records ΔPWV images at 10 min increments. While the grating structure embedded in the planar PC is aligned along the vertical direction on the PWV images, many cells orient themselves in other directions, including directly perpendicular to the grating lines as shown in Figure 4. The spreading and migration directions of the cells appear to be significantly more random than the nonplanar sensor. Patterns in Figure 4 are representative of at least three independent experiments. Video S3 (Supporting Information) shows the adhesion and migration processes of the 3T3 fibroblast cells that are imaged with a different planar PC surface every 15 min for 10 h. The observation of cell activities is consistently in terms of the lack of directional movement. To further demonstrate the difference between the morphology of the cells on planar and nonplanar PC surfaces during the attachment process, the evolution of the cell boundary in the two long-term scans is tracked and presented in **Figure 5**. Figure 5a characterizes the change of the contour of a cell (shown at position "a" in Figure 3) on the planar PC surface. The round pattern of the initial attachment gradually transforms into a long narrow region stretched along the grating direction. The cell spreading pattern in Figure 5b, on the other hand, shows the cells (shown at position "b" in Figure 4) align and extend themselves in an unbiased manner. Compared with the cells on nonplanar PC, the contours of cells on planarized PCs are more nonspecific, and the spreading directions of the cells proceed in all directions, not just along the grating structure, as observed on the nonplanar sensors.

3. Discussion and Conclusion

The study of the interaction between cells and their extracellular environment is critical for understanding the fundamental

Adv. Optical Mater. 2015,
DOI: 10.1002/adom.201500260

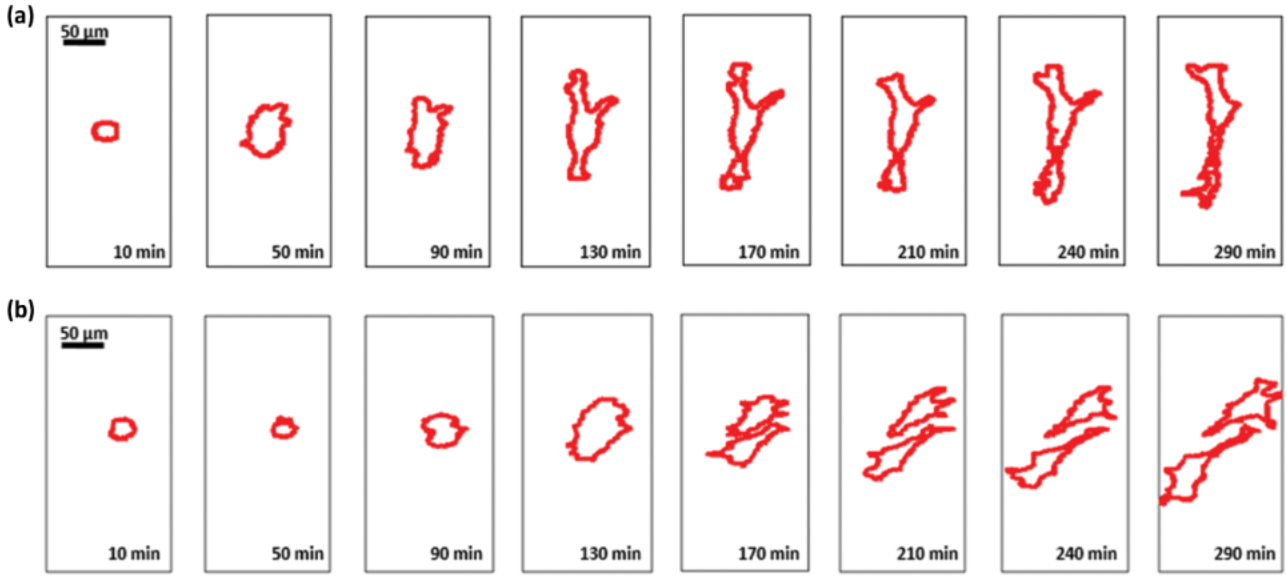

Figure 5. Comparison of the contour evolution of a selected cell attached to a) the nonplanar and b) the planar PC surface. Part (a) tracks the boundary evolution of a cell (marked with "a" on Figure 3) on the nonplanar PC surface, where the initial round pattern gradually becomes stretched along the grating direction (vertical). Part (b) shows the unbiased spreading of cells (marked with "b" on Figure 4) on the planar PC surface.

mechanisms through which cells communicate with their immediate environment. It has been demonstrated that surface topography in the nanometer and micrometer regimes plays a significant role in regulating many complex biological processes such as stem cell differentiation and tissue organization. Many types of cells, especially mammalian cells, exhibit modulated cellular morphology and biased migration directions while they are cultured on micro- and nanoscale topographic structures, such as periodic grooves, pillars, and pits. While label-free biosensors have emerged to perform noninvasive detection of cell activities without the use of fluorescent labels, they often employ surface structures with specific topographic patterns to probe cell–surface interactions. To date, little effort has been done on understanding the potential effects of these nanopatterned structures on the morphology of cellular attachment and spreading. Here we provide both evidence of grating-directed cellular growth on a traditional PC structure and the elimination of the behavior with a planar surface PC. As many uses for label-free detection methods are directed at understanding processes of cell–substrate interaction, providing a neutral, unbiasing substrate while maintaining the label-free optical properties is an important achievement for the realm of PC biosensing. Our results demonstrate that planarization should optimally be performed with the thinnest possible layer to preserve optical coupling of the surface-confined electrical field with the detected cells.

In this work, a fabrication approach that combines nanoreplica molding and a horizontal dipping process has been implemented to produce a PC biosensor with a planar surface. Nanoreplica molding allows for the accurate transfer of grating patterns from a molded template to a UV-curable polymer layer with submicron accuracy onto low-cost glass coverslips that can be easily incorporated into commonly used microscope slides or microplates used for a variety cell studies. The grating period and TiO_2 thickness are chosen to maximize label-free sensitivity while ensuring spectral overlap with the illumination source (LED with peak wavelength at 617 nm) near normal incidence. The output of the LED can provide low power, noncoherent and visible illumination for the imaging of live cells. The horizontal dipping process is capable of covering grating structures within a precisely controlled thin-film polymer layer via capillary action. Although the fabrication processes are completed in a laboratory environment, all methods described herein can easily be adapted within a roll-to-roll manufacturing paradigm. In order to verify the surface planarity, the surface characteristics of the planar PC are analyzed by AFM and spectroscopic measurements. RCWA computer simulation is also applied to model the optical properties of the planar PC. By virtue of the evanescent waves generated by resonant optical coupling at the PC surface, the planar PC is able to detect the cell behaviors specifically at the cell–PC interface. Label-free images of 3T3 fibroblast cells adhering and spreading filopodia across the planar and nonplanar PC are captured using the PCEM system over a 5 h period. As expected, the planar surface effectively eliminates the directionally biased cellular attachment behaviors that are usually observed on nanopatterned structures. The evolution of cell morphology during the attachment and spreading processes is studied, and the preferential orientation and extension of cellular processes observed on typical PC sensors is eliminated when the new, planar sensors are used.

The label-free cell imaging provided by planar PCs is a promising tool for a number of cellular biology studies including tissue engineering, drug screening, and many other clinical applications. While the PC surface in this experiment is coated with fibronectin to facilitate cell adhesion upon the surface, the process can easily be adapted to a variety of other ECM proteins to mimic a variety of extracellular environments, enabling the study of many cellular responses in vitro without the use of fluorescent labels or substrate contact guidance. Here, the work presents an important step forward in developing truly

label-free techniques for observing cellular processes without unintended external environmental modulation. Cell migration and invasion assays[51] can be performed on the new, planar surface provided by this sensing platform, which will further improve the existing tools used for the efficient identification of valuable compounds and timely recognition of undesirable effects of the drug discovery process by eliminating an outside source of directional bias. The planar PC biosensor is compatible with most common microscopy techniques used in cell biology due to the glass slide-based fabrication method and wide spectral tunability of the resonant wavelength.

4. Experimental Section

Planar PC Fabrication: The fabrication process for the planar PC biosensor is illustrated in **Figure 6**. The planar PC was comprised of a subwavelength grating structure of periodically arranged low and high refractive index materials and a flat polymer coating that filled the grating gaps. The grating was formed in a layer of ultraviolet-curable polymer (UVCP) on top of a flexible glass coverslip through an approach called "nanoreplica molding" (Figure 6a). In this approach, a quartz molding template with a negative volume image of the desired grating structure (period = 400 nm, duty cycle = 50%, depth = 120 nm) was fabricated using electron beam lithography and reactive ion etching. A small volume of liquid UV-curable epoxy was squeezed between a glass cover slip (0.17 mm thick) and the template, which was subsequently cured to a rigid solid state using a high-intensity UV lamp. The solidified UVCP preferentially adhered to the glass substrate and was peeled away from the quartz template, leaving a replica of the grating mold on the glass cover slip. The PC grating area was 0.9 × 0.9 cm. An initial thin film of TiO_2 ($t \approx 40$ nm) was deposited via reactive radio frequency (RF) sputtering (PVD 75, Kurt Lesker) providing the high refractive index coating (Figure 6b). The grating height after the TiO_2 deposition was ≈105 nm, as measured by atomic force microscope (Figure 1a).

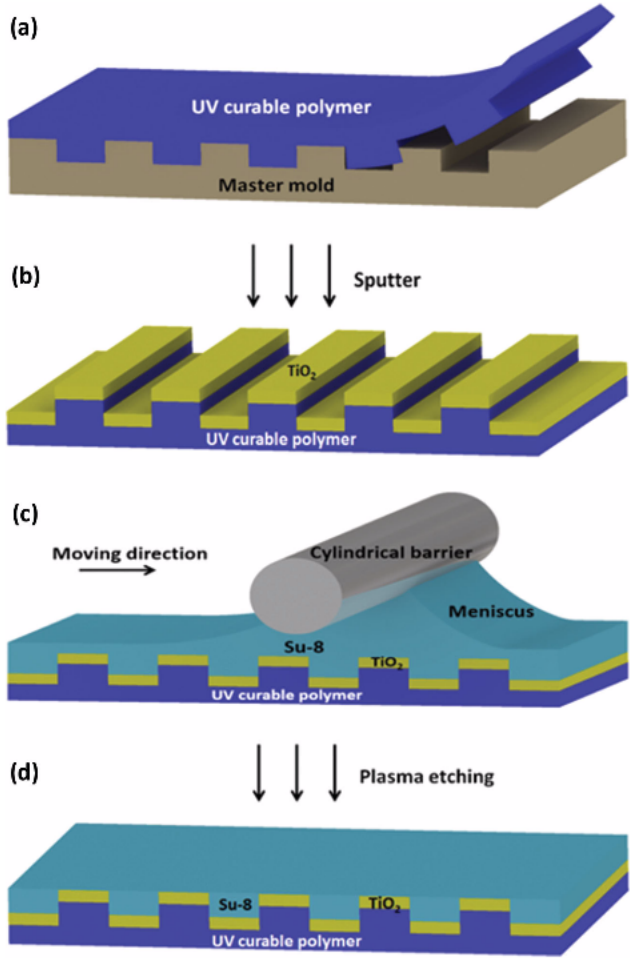

Figure 6. Fabrication process of the planar PC biosensor. a) The fabrication begins with nanoreplica molding of the subwavelength grating structures from the master mold to the UV-curable polymer layer. b) After the UV-curable polymer layer is peeled off from the master mold, sputter deposition is applied to coat a high refractive index TiO_2 film on top of the grating. c) Next, the horizontal dipping process flattens the grating surface by embedding the grating into a thin film of SU-8 polymer. d) A plasma etchback treatment is followed to reveal the grating top surface. A thin film of TiO_2 is deposited on top of the planar PC as the final step.

The horizontal dipping process was subsequently applied to flatten the grating structure through the coating of a thin film of SU-8 polymer. SU-8 was selected as the coating material for several reasons. First, SU-8 is one of the most commonly used epoxy-based photoresists that can be easily cured by UV light exposure. Second, the low viscosity of SU-8 solution (20 wt%) can provide a submicron film coating thickness by horizontal dipping. Third, SU-8 has a high optical transmission efficiency at wavelengths above 360 nm. Finally, SU-8 has demonstrated a high degree of cell biocompatibility.[44] Before the process, SU-8 solution was prepared by mixing SU-8 2000.5 with SU-8 thinner (Microchem Corporation) at a volume ratio of 1:4. The mixed solution was sonicated for 1 min for homogenization. A schematic illustration of the coating process is shown in Figure 1c. The core component of the custom-built horizontal dipping system was a translatable coating barrier, comprised of a stainless steel cylindrical rod (Thorlabs Inc.) with a diameter of 0.5 in. and a length of 4 in. The coating barrier was mounted on a 2D (x and z) translation stage, with the vertical stage placing the barrier at a height of $h_0 = 1.2$ mm with respect to the PC surface. The PC was firmly held onto a porous vacuum chunk (Wenesco Inc.) from below. After injection of ≈100 µL of the SU-8 solution into the narrow gap between the coating barrier and the PC surface, a downstream meniscus of the solution was formed by attraction to the coating barrier via capillary action. The coating barrier was then transported horizontally at a constant speed of 0.1 cm s^{-1} controlled by a motorized stage (Sigma Koki Co.) to draw the meniscus from the front edge of the PC surface to the back edge, leaving a thin film of the SU-8 solution evenly spread on top of the grating substrate. Due to the surface tension within the SU-8 solution, the coating film could maintain an unstructured plane at the top. After horizontal dipping, the coated PC was soft baked at 65 °C for 3 min and 95 °C for 30 min to remove the excess solvent. Next, the SU-8 film was photopolymerized by exposure to a high power xenon UV lamp (RC-600, Xenon Co.) for 20 s, and subsequently hard baked on a 95 °C hotplate for an additional 30 min. After the baking process, the grating structure was completely embedded within the polymer layer with a planar surface. To etch away the extra polymer on top of the grating tooth structure, a short (≈30 s) oxygen plasma treatment was applied to the PC under the condition of 150 mTorr pressure and 250 W RF power. The oxygen plasma etch rate was deliberately slow, so as to accurately control the etched depth, resulting in an SU-8 film that filled in the grating teeth, but that left only 0–5 nm of SU-8 covering the top of the PC teeth. The final fabrication step was deposition of a 10 nm thick layer of TiO_2 over the horizontal-dipped layer via reactive RF sputtering. The TiO_2 film served two purposes. It provided a metal oxide surface that was consistent with various forms of surface functionalization that were used for SiO_2 or TiO_2 biosensors, and its high refractive index served to bias the resonant electric field of the PC more fully into the liquid media, thus improving sensitivity.

Detection Instrument: A schematic diagram of the PCEM instrument is shown in Figure S2 (Supporting Information). The system was built upon the body of a standard microscope (Carl Zeiss Axio Observer Z1),

Adv. Optical Mater. **2015**,
DOI: 10.1002/adom.201500260

but in addition to ordinary bright field imaging, a second illumination path was provided from a fiber-coupled broadband light-emitting diode (LED) (Thorlabs M617F1, $600 < \lambda < 650$ nm). The fiber output was collimated by an air-spaced doublet collimator and filtered by a polarizing beamsplitter cube to provide a linearly polarized beam of light. The polarized beam was focused by a cylindrical lens ($f = 200$ mm) to form a linear beam at the back focal plane of the objective lens (10×, Zeiss). After passing through the objective lens, the orientation of the line-shaped beam was rotated to illuminate the PC from below at normal incidence, with its electric field vector oriented perpendicular to the grating lines of PC. The reflected light was projected, via a side port of the inverted microscope and a zoom lens, onto a narrow slit aperture at the input of an imaging spectrometer. The width of the adjustable slit was set to 30 μm for the work reported here. Using this method, reflected light was collected from a line that spanned the PC surface, where the width of the imaged line, 1.2 μm, was determined by the width of the entrance slit of the imaging spectrometer and the magnification power of the objective lens. The system incorporated a grating-based spectrometer (Acton Research) with a 512 × 512 pixel charge-coupled device (CCD) camera (Photometrics Cascade 512). The line of reflected light, containing the resonant biosensor signal, was diffracted by the grating within the spectrometer (300 lines mm^{-1}) to produce a spatially resolved spectrum for each point along the line. Therefore, each pixel across the line was converted to a resonant reflection spectrum, containing a narrow bandwidth reflectance peak from the PC. The PWV of each peak was determined by fitting the spectrum to a second-order polynomial function, and then mathematically determining the maximum wavelength of the function. By fitting all 512 spectra, in a process that took 20 ms, a line comprised of 512 pixels was generated that represented one line of a PWV image of the PC surface. With an effective magnification of 26×, each pixel in the line represented an ≈0.6 μm region of the PC surface and 512 such pixels covered a total width of ≈300 μm. To generate a 2D PWV image of the PC surface, a motorized stage (Applied Scientific Instruments, MS2000) translated the sensor along the axis perpendicular to the imaged line in increments of 0.6 μm per step. Using this technique, a series of lines were assembled into an image at a rate of 0.1 s per line and the same area on the PC surface could be scanned repeatedly. Each image was comprised of 512 by n pixels, where n could be selected during each scan session, and each pixel represents a 0.6 × 0.6 μm region of the PC surface.

Cell Culture and Sensor Preparation: The 3T3 fibroblasts (ATCC) were cultured in dulbecco's modified eagle medium (DMEM) with 5% fetal bovine serum. Silicone rubber gaskets (prepared using polydimethylsiloxane) with an internal area of 1.0 × 1.0 cm^2 were attached to the sensor surface to provide media containment (1 mL volume). Prepared slides were sonicated for 1 min in acetone, followed by cleaning with isopropyl alcohol (IPA) and water. After thorough drying with N_2, the PC biosensor was treated with oxygen plasma and incubated with 10 mg mL^{-1} fibronectin to encourage cell attachment. Imaging was completed on the instrument as described above with the microscope stage enclosed within an environmentally controlled incubation chamber (Zeiss) maintaining constant 37 °C temperature and 5% CO_2.

Supporting Information

Supporting Information is available from the Wiley Online Library or from the author.

Acknowledgements

The authors are grateful for the funding support provided by National Science Foundation (NSF CBET 11-32301) and the NCI Alliance for Nanotechnology in Cancer Midwest Cancer Nanotechnology Training Center (NIH Grant R25 CA154015A) for this work. Additionally, this work was also partially supported by Jeongsong Cultural Foundation. Any opinions, findings, and conclusions or recommendations in this work are those of the authors and do not necessarily reflect the views of the National Science Foundation.

Received: May 11, 2015
Revised: July 30, 2015
Published online:

[1] M. Barczyk, S. Carracedo, D. Gullberg, *Cell Tissue Res.* **2010**, *339*, 269.
[2] J. Boudreau, P. L. Jones, *Biochem. J.* **1999**, *339*, 481.
[3] K. M. Yamada, *Ann. Rev. Biochem.* **1983**, *52*, 761.
[4] A. Zoumi, A. Yeh, B. J. Tromberg, *Proc. Natl. Acad. Sci. USA* **2002**, *99*, 11014.
[5] P. Friedl, *Histochem. Cell Biol.* **2004**, *122*, 183.
[6] W. J. Rosoff, J. S. Urbach, M. A. Esrick, R. G. McAllister, L. J. Richards, G. J. Goodhill, *Nat. Neurosci.* **2004**, *7*, 785.
[7] B. T. Cunningham, P. Li, S. Schulz, B. Lin, C. Baird, J. Gerstenmaier, C. Genick, F. Wang, E. Fine, L. Laing, *J. Biomol. Screening* **2004**, *9*, 481.
[8] F. Vollmer, S. Arnold, *Nat. Methods* **2008**, *5*, 591.
[9] J. S. Daniels, N. Pourmand, *Electroanalysis* **2007**, *19*, 1239.
[10] D. W. Unfricht, S. L. Colpitts, S. M. Fernandez, M. A. Lynes, *Proteomics* **2005**, *5*, 4432.
[11] W. Wang, Y. Z. Yang, S. P. Wang, V. J. Nagaraj, Q. Liu, J. Wu, N. J. Tao, *Nat. Chem.* **2012**, *4*, 846.
[12] M. Varshney, Y. Li, *Biosens. Bioelectron.* **2009**, *24*, 2951.
[13] A. W. Peterson, M. Halter, A. Tona, K. Bhadriraju, A. L. Plant, *BMC Cell Biol.* **2009**, DOI:10.1186/1471-2121-10-16.
[14] K. J. Moh, X. C. Yuan, J. Bu, S. W. Zhu, B. Z. Gao, *Opt. Express* **2008**, *16*, 20734.
[15] W. Wang, S. P. Wang, Q. Liu, J. Wu, N. J. Tao, *Langmuir* **2012**, *28*, 13373.
[16] W. L. Chen, K. D. Long, M. Lu, V. Chaudhery, H. Yu, J. S. Choi, J. Polans, Y. Zhuo, B. A. Harley, B. T. Cunningham, *Analyst* **2013**, *138*, 5886.
[17] Y. Zhuo, H. Hu, W. L. Chen, M. Lu, L. M. Tian, H. J. Yu, K. D. Long, E. Chow, W. P. King, S. Singamanenic, B. T. Cunningham, *Analyst* **2014**, *139*, 1007.
[18] B. Cunningham, P. Li, B. Lin, J. Pepper, *Sens. Actuators B: Chem.* **2002**, *81*, 316–328.
[19] S. George, I. D. Block, S. I. Jones, P. C. Mathias, V. Chaudhery, P. Vuttipittayamongkol, H. Y. Wu, L. O. Vodkin, B. T. Cunningham, *Anal. Chem.* **2010**, *82*, 8551.
[20] H. Shafiee, E. A. Lidstone, M. Jahangir, F. Inci, E. Hanhauser, T. J. Henrich, D. R. Kuritzkes, B. T. Cunningham, U. Demirci, *Sci. Rep.* **2014**, DOI: 10.1038/srep04116.
[21] C. Ge, M. Lu, S. George, T. A. Flood, C. Wagner, J. Zheng, A. Pokhriyal, J. G. Eden, P. J. Hergenrotherd, B. T. Cunningham, *Lab Chip* **2013**, *13*, 1247.
[22] H. Y. Wu, C. J. Choi, B. T. Cunningham, *Small* **2012**, *8*, 2878.
[23] E. A. Lidstone, V. Chaudhery, A. Kohl, V. Chan, T. Wolf-Jensen, L. B. Schook, R. Bashir, B. T. Cunningham, *Opt. Express* **2009**, *17*, 13222.
[24] I. D. Block, P. C. Mathias, S. I. Jones, L. O. Vodkin, B. T. Cunningham, *Analyst* **2011**, *136*, 3608.
[25] I. D. Block, P. C. Mathias, S. I. Jones, L. O. Vodkin, B. T. Cunningham, *Appl. Opt.* **2009**, *48*, 6567.
[26] B. Lin, P. Li, B. T. Cunningham, *Sens. Actuators B: Chem.* **2006**, *114*, 559.
[27] L. L. Chan, S. L. Gosangari, K. L. Watkin, B. T. Cunningham, *Apoptosis* **2007**, *12*, 1061.
[28] S. M. Shamah, B. T. Cunningham, *Analyst* **2011**, *136*, 1090.

[29] P. Clark, P. Connolly, A. S. G. Curtis, J. A. T. Dow, C. D. W. Wilkinson, *Development* **1990**, *108*, 635.
[30] P. Clark, P. Connolly, A. S. G. Curtis, J. A. T. Dow, C. D. W. Wilkinson, *Development* **1987**, *99*, 439.
[31] K. Kulangara, K. W. Leong, *Soft Matter* **2009**, *5*, 4072.
[32] M. Nikkhah, F. Edalat, S. Manoucheri, A. Khademhosseini, *Biomaterials* **2012**, *33*, 5230.
[33] C. J. Bettinger, R. Langer, J. T. Borenstein, *Angew. Chem. Int. Ed.* **2009**, *48*, 5406.
[34] S. A. Biela, Y. Su, J. P. Spatz, R. Kemkemer, *Acta Biomater.* **2009**, *5*, 2460.
[35] X. F. Walboomers, J. A. Jansen, *Odontology* **2001**, *89*, 0002.
[36] R. Flemming, C. Murphy, G. Abrams, S. Goodman, P. Nealey, *Biomaterials* **1999**, *20*, 573.
[37] C. S. Chen, M. Mrksich, S. Huang, G. M. Whitesides, D. E. Ingber, *Science* **1997**, *276*, 1425.
[38] J. Lee, A. A. Abdeen, T. H. Huang, K. A. Kilian, *J. Mech. Behav. Biomed. Mater.* **2014**, *38*, 209.
[39] K. K. Parker, D. E. Ingber, *Phil. Trans. R. Soc. B: Biol. Sci.* **2007**, *362*, 1267.
[40] J. M. Steigerwald, S. P. Murarka, R. J. Gutmann, *Chemical Mechanical Planarization of Microelectronic Materials*, John Wiley & Sons, NY, **2008**.
[41] L. E. Stillwagon, R. G. Larson, G. N. Taylor, *J. Electrochem. Soc.* **1987**, *134*, 2030.
[42] Y. F. Tan, C. Ge, A. Chu, M. Lu, W. Goldshlag, C. S. Huang, A. Pokhriyal, S. George, B. T. Cunningham, *IEEE Sens. J.* **2012**, *12*, 1174.
[43] B. Park, M. Y. Han, *Opt. Express* **2009**, *17*, 21362.
[44] K. V. Nemani, K. L. Moodie, J. B. Brennick, A. Su, B. Gimi, *Mater. Sci. Eng. C: Mater. Biol. Appl.* **2013**, *33*, 4453.
[45] I. D. Block, N. Ganesh, M. Lu, B. T. Cunningham, *IEEE Sens. J.* **2008**, *8*, 274.
[46] W. L. Chen, K. D. Long, H. J. Yu, Y. F. Tan, J. S. Choi, B. A. Harley, B. T. Cunningham, *Analyst* **2014**, *139*, 5954.
[47] M. T. Frey, I. Y. Tsai, T. P. Russell, S. K. Hanks, Y. L. Wang, *Biophys. J.* **2006**, *90*, 3774.
[48] Y. Fang, *Int. J. Electrochem.* **2011**, 2011.
[49] R. Schroder, J. Schmidt, S. Blattermann, L. Peters, N. Janssen, M. Grundmann, W. Seemann, D. Kaufel, N. Merten, C. Drewke, J. Gomeza, G. Milligan, K. Mohr, E. Kostenis, *Nat. Protocols* **2011**, *6*, 1748.
[50] R. J. Pelham, Y. L. Wang, *Proc. Natl. Acad. Sci. USA* **1997**, *94*, 13661.
[51] K. I. Hulkower, R. L. Herber, *Pharmaceutics* **2011**, *3*, 107.

Adv. Optical Mater. **2015**,
DOI: 10.1002/adom.201500260